Electronic structure of the water dimer cation

Piotr A. Pieniazek[a], Joost VandeVondele[b], Pavel Jungwirth[c*],
Anna I. Krylov[a*], Stephen E. Bradforth[a*]

[a] Department of Chemistry, University of Southern California, Los Angeles, CA 90089-0482, USA

[b] Physical Chemistry Institute, Zurich University, Winterthurerstrasse 190, CH-8057 Zurich, Switzerland

[c] Institute of Organic Chemistry and Biochemistry, Academy of Sciences of the Czech Republic,
and Center for Biomolecules and Complex Molecular Systems,
Flemingovo nám. 2, 16610 Prague 6, Czech Republic

March 11, 2008

Abstract

The spectroscopic signatures of proton transfer in the water dimer cation were investigated. The six lowest electronic states were characterized along the reaction coordinate using the equation-of-motion coupled-cluster method with single and double substitutions for ionized systems. The nature of the dimer states was explained in terms of the monomer states using a qualitative molecular orbital framework. We found that proton transfer induces significant changes in the electronic spectrum, thus suggesting effective use time-resolved electronic femtosecond spectroscopy to monitor the dynamics following ionization. The electronic spectra at vertical and proton-transferred configurations include both local excitations (features similar to those of the monomers) and charge-transfer bands. *Ab initio* calculations were used to test the performance of a self-interaction correction for density functional theory (DFT). It is found that the corrected DFT/BLYP method is capable of reproducing the correct ordering of the $(H_2O)_2^+$ isomers, and thus may be employed in calculations of larger systems.

1 Introduction

Ionized states in condensed media, for example, those produced by radiation in biological tissue, or encountered in the storage and reprocessing of fissioned nuclear materials are not yet fully understood.[1–3] Even radiolysis of water, a predominant molecular target of the incident radiation in these situations, which has also served as the prototypical system for disentangling the phenomenology of high energy processes in bulk liquids, has not been completely mapped out. For example, both the nature of the initially excited states and sub-50 fs ionization/dissociation dynamics after deposition of energy have not been directly observed.[3]

The major ionization channel in water radiolysis includes the following steps:

$$n\ H_2O \rightarrow (H_2O)_n^* \rightarrow H_2O^+(H_2O)_{n-1} + e^- \rightarrow \ldots \rightarrow H_3O^+_{aq} + OH_{aq} + e^-_{aq} \qquad (1)$$

The extent of delocalization of the initial excitation, i.e., the number n of water molecules participating in $(H_2O)_n^*$, and the character of the charged species immediately after charge separation are poorly defined. Both quantities are likely to depend on the initial energy deposited.[4] In addition to reaction (1), energy deposited into water can also lead to homolytic bond breaking yielding H + OH, which resembles the gas phase photodissociation.[5] Beside the practical interest in the yields and spatial distribution of reactive radical products, this system also presents several fundamental questions on the mechanism and dynamics of separation and delocalization of both charge and spin in a partially disordered and rapidly fluctuating system.

Both the electronic structure and molecular dynamics of water are amenable to simulation. While the structure, dynamics and spectroscopy of the excess electron have been extensively investigated, modeling the other initial product of photoionization,[6,7] the ionized hole, has not been attempted in bulk, although cluster studies were reported.[8–11] The delocalization of the initial charge, the timescale and dynamics of reaction (1), as well as the the fate and separation of the products are all important issues which a simulation could help to explain. Our ongoing efforts to simulate the excess hole in bulk require the benchmarking of electronic structure methods for *ab initio* molecular dynamics (AIMD). One of the goals of the present study is to compare reliable calculations of the simplest fragment of the hole in water, the water dimer cation, against less computationally demanding methods suitable for AIMD.[12]

Moreover, in the laboratories of one of us, photolysis studies of pure water have been carried out with pulses as short as 25 fs. With this time resolution, femtosecond pump-probe spectroscopy should be able to track the proton transfer step in reaction (1) and with a dispersed probe covering continuously the near UV and visible, the transients should be identifiable by their spectroscopic signatures. However, it is critical to establish the signature of the H_2O^+ intermediate and distinguish it from the subsequent species such as (OH-H_3O^+) and OH_{aq}.[13,14] Therefore, another major goal of this work is to accurately describe the excited states of each of these species, at least at the level of small clusters. This will allow an assessment of what information electronic spectroscopy can provide in tracking the ionization chemistry of bulk water.

Our theoretical approach parallels a recent study we performed on the electronic spectroscopy of the benzene dimer cation, a core species in ionization of liquid benzene.[15] The results for a gas phase water dimer establish a foundation for understanding the ionized water in the condensed phase. Moreover, the gas phase species is also of interest and has attracted experimental and theoretical attention in the past, albeit not in the the context of its electronic spectroscopy. Ng et al.[16] determined the adiabatic ionization energy (IE) to be 11.2 eV by photoionization threshold measurements. De Visser[17] and coworkers investigated the reactivity of $(H_2O)_2^+$ towards a series of substrates, placing the adiabatic IE in the 10.8 - 10.9 eV bracket. Achiba and coworkers[18] measured the photoelectron spectra of $(H_2O)_2^+$ providing information about the two lowest electronic states of the cation. They observed two broad peaks centered at 12.1 and 13.2 eV, and determined the onset of ionization to be at 11.1 eV. This work spurred a series of theoretical studies.[19–25] While the first ionization was assigned as ionization from the out-of-plane orbital of the donor molecule, there was a controversy as to the site of second ionization. Early study pointed to ionization of the a_1 donor orbital, but subsequent correlated calculations reassigned it to the b_1 acceptor orbital.[23] Also, 2D potential energy surface (PES) cuts for the proton transfer reaction along the O-O and O-H coordinates were calculated.[22] Density functional theory (DFT) calculations determined the lowest-energy isomer to be the hemibonded structure,[26,27] which later was shown to be

an artifact of the self-interaction error (SIE).[28] Müller and coworkers studied ionization of small water clusters using Green's functions.[29] Their work focused on vertical structures and a hinted at delocalized nature of the hole in the ground and excited states of water cluster cations.

This work presents calculations for the water dimer cation at the geometry of the neutral water dimer and along the proton transfer reaction coordinate to the OH–H_3O^+ products. The character of the ground and the low-lying excited states are described within a Dimer Molecular Orbital - Linear Combination of Fragment Molecular Orbitals (DMO-LCFMO) framework. We also chart the electronic spectroscopy of the system as it evolves along the reaction coordinate. The predictions of this study will help guide ongoing laboratory femtosecond studies and AIMD simulations of ionized bulk water.

2 Theoretical methods and computational details

We begin by characterizing the monomer fragments and then proceeded to the structures and excited states of water dimer cation. Proper description of the ground and excited electronic states of doublet systems, like $(H_2O)_2^+$ or OH, is problematic due to symmetry breaking and spin-contamination of the doublet Hartree-Fock (HF) references.[30–32] Equation-of-motion coupled-cluster for ionization energies (EOM-IP-CC)[33–36] overcomes these difficulties by describing the problematic open-shell doublet wave functions $\Psi(cation)$ as ionized/excited states of a well-behaved neutral wave function $\Psi(neutral)$:

$$\Psi(cation) = \hat{R}\Psi(neutral), \tag{2}$$

where the Koopmans-like operators R generate all possible ionized and ionized and excited configurations out of the closed-shell reference determinant, and $\Psi(neutral)$ is a coupled-cluster wave function, typically including only single and double substitutions (CCSD). Truncating R at $1h2p$ and $2h3p$ levels gives rise to the EOM-IP-CCSD and EOM-IP-CC(2,3) models.

The geometries of the closed-shell species [H_2O, OH^-, H_3O^+, $(H_2O)_2$] were optimized at the second-order Møller-Plesset perturbation theory level with the 6-311++G** basis set (MP2/6-311++G**), while those of the open-shell doublet species [OH, proton-transferred and hemibonded $(H_2O)_2^+$] — at the EOM-IP-CCSD/6-311++G** level. In the case of the proton-transferred structure both the C_s and the C_1 symmetry structures were obtained. Monomer calculations of IEs were carried out, and their accuracy was assessed using the available experimental data. Calculations were performed at the EOM-IP-CCSD and EOM-IP(2,3)-CC levels using the 6-311++G** and aug-cc-pVTZ basis sets. Based on these benchmark results, the 6-311++G** basis set was selected for production calculations. Excitation energies and transition properties for monomer fragments and the dimer were computed using EOM-IP-CCSD and EOM-CCSD for excitation energies (EOM-EE-CCSD).[37–39] Additionally, excitation energies were obtained using EOM-IP-CC(2,3). The character of the dimer excited states was characterized using the Natural Bond Orbital (NBO) analysis[40] by calculating the natural charge of the fragments. The NBO analysis was also applied to the reference CCSD/6-311++G** wave functions. When appropriate, unrestricted HF (UHF) references were used in geometry optimizations, and restricted open-shell (ROHF) references employed in evaluation of excitation energies and transition properties.

To characterize the proton transfer reaction from the vertical ionized dimer, we computed a PES scan using EOM-IP-CCSD/6-311++G**, under the C_s symmetry constraint. To evaluate the consequences of this approximation, we compared C_1 and C_s configurations of the proton-transferred structure. Briefly, excitation energies are insensitive to this constraint, but intensities are. The distance between the oxygen atoms was varied between 2.30 Å and 3.10 Å, while the distance between the hydrogen of the H-bond donor and the oxygen of the acceptor was varied from 0.90 Å to 2.20 Å, with 0.05 Å increments. At each point a constrained geometry optimization was conducted. Subsequently, the points corresponding to the neutral (A) and proton-transferred geometries (C) were identified on the grid. A steepest descent path was followed between A and C. Excitation energies and transition properties were computed along the path using EOM-IP-CCSD/6-311++G**.

All *ab initio* calculations were performed using the *Q-CHEM ab initio* package.[41] The basis sets were obtained from the EMSL repository.[42] The geometries are available as supplementary material.

With the goal of *ab initio* Born-Oppenheimer molecular dynamics simulations of photoionization in bulk water,[12] we benchmarked the performance DFT methods implemented within the *CP2K/Quickstep* software package.[43] In *CP2K/Quickstep*, DFT is implemented using a mixed Gaussian and plane-waves approach. We employed the BLYP functional with the double-zeta (DZVP) and the triple-zeta (TZV2P) basis sets, along with the Goedecker-Teter-Hutter pseudo-potentials for oxygen 1s electrons.[44] The energy cutoff for plane waves was set to 280 Ry. Calculations for the radical cation were performed using unrestricted (UKS) and restricted open-shell (ROKS) Kohn-Sham schemes. To eliminate the errors due to electron self-interaction,[45–47] which are significant for open-shell and charge-transfer systems, we applied a self-interaction correction (SIC) within the ROKS method.[48–50] For SIC we used the recommended values of 0.2 for Coulomb term scaling and zero for scaling of the exchange-correlation term.[49] For comparison and a stability check we also employed the value of 0.2 for the latter scaling.

3 Results

3.1 Monomers

The DMO-LCFMO description (see Appendix) of the dimer is based on the fragment orbitals and relevant excited states. In the water dimer cation, we are interested in the states derived by single ionization of the neutral. Thus, at the vertical geometry the DMOs can be expressed in terms of the occupied H_2O orbitals. The proton-transferred cation orbitals originate from the OH^- – H_3O^+ dimer, and the OH^- and H_3O^+ occupied orbitals form a neutral basis. The three highest occupied molecular orbitals (MOs) of H_2O, OH^-, and H_3O^+ are shown in Fig. 1, and the corresponding IEs are given in Table 1. Overall, the theory and the experiment, where available, agree well.

It is important to determine which of the monomer transitions are relevant to the dimer cation spectroscopy. The ground-state electronic structure at the proton-transferred geometry corresponds to the ionization of the hydroxyl part of the OH^- – H_3O^+ dimer, as dictated by the IE considerations. The EOM-IP method restricts us to the electronic states derived by single ionizations of the neutrals. Thus, we only discuss transitions in the ionized system

for which the singly occupied MO (SOMO) is the target orbital. This restricts the types of transitions to: (i) the transitions within the OH moiety, (ii) the transitions from the H_3O^+ to the OH moiety leading to the formation of OH^- – H_3O^{2+}. The two groups can be related to the excited states of OH and H_3O^{2+} molecules, respectively. In contrast, excitations at the neutral vertical geometry always correspond to H_2O^+ – H_2O, the charge being located either on the H-bond donor or the acceptor. Thus, one needs to consider only the states of H_2O^+. The excited states of monomers are given in Table 2.

There are two possible excitations in H_2O^+ in the relevant energy range. The $b_1 \leftarrow a_1$ transition is optically allowed and occurs at 2.3 eV, while the dipole forbidden $b_1 \leftarrow b_2$ excitation is at 6.5 eV. The character of the electronic states does not change upon structural relaxation from the vertical neutral to the cation geometry. The OH radical has only one excitation, $\pi \leftarrow \sigma$, at 4.2 eV. Addition of a proton to H_2O^+ produces H_3O^{2+}, which features a weak $a_1 \leftarrow e$ transition at 5.8 eV. Overall, addition/subtraction of a proton to/from H_2O^+ dramatically changes the nature of the MOs and the electronic transitions. Thus, each species has unique electronic states that cannot be described as perturbed H_2O^+ states.

The EOM-IP-CCSD method treats accurately the dimer cation states derived by single ionization of the neutrals, while the cation states corresponding to excitation to a virtual orbital of the neutral are not well described owing to their significant two-electron character. This is acceptable only when these states are outside the experimentally relevant spectral region (1 – 6 eV). In the context of the water dimer cation at the geometry of the neutral species, we need to consider the excited states of H_2O^+ and H_2O. The lowest excited state of water monomer in the gas phase is the $\tilde{A}\ ^1B_1$ state at 7.4-7.5 eV.[51] It is derived by excitation from the $1b_1$ to the $4a_1$/Rydberg $3s$ orbital. The first two excitations (2 and 6 eV) in H_2O^+ are excitations to SOMO, and are well described by EOM-IP-CCSD. The next excited state, $2\ ^2B_1$, occurs at 13.7 eV as calculated by EOM-EE-CCSD/6-311++G**. At the proton-transferred configuration states of H_3O^+ and OH are relevant. The lowest excited state of H_3O^+, $2\ ^1A_1$, occurs at 11.8 eV (EOM-EE-CCSD/6-311++G**). The lowest OH excitation is $\sigma \leftarrow \pi$ at 4 eV and is described by EOM-IP-CCSD. The next one, to the B $^2\Sigma^+$ state, is at 8.7 eV. Thus, monomer states that not described by EOM-IP-CCSD are well outside the region probed in the experiment, both at the neutral and at the proton-transferred geometry.

3.2 Dimers

3.2.1 Ground state geometry

The structures of $(H_2O)_2^+$ considered in this work are shown in Fig. 2. The neutral structure has C_s symmetry with the oxygen atoms separated by 2.91 Å. This geometry is not a stationary point on the cation PES and provides time-zero reference for the structure prepared by time-resolved spectroscopy. IEs and MOs at this geometry are shown in Fig. 3. EOM-IP-CCSD and EOM-IP-CC(2,3) predict the vertical IE to be 11.4 and 11.3 eV, respectively. This is lower than the experimental value of 12.1 eV.[18] The adiabatic IE was determined experimentally to lie in the range 10.8 - 11.2 eV.[16–18] The equivalent energy gap (not including zero-point energy differences) computed using EOM-IP-CCSD and EOM-IP-CC(2,3) is 10.55 and 10.40 eV, respectively.

Ionization facilitates the downhill barrierless proton transfer from the H-bond donor to the acceptor, leading to the formation of OH – H_3O^+ (Fig. 2b). Electronically, these products

correlate with the OH^--H_3O^+ state of the neutral. There is a large geometric change associated with the proton transfer as the oxygen-oxygen distance decreases to 2.47 Å and the symmetry is lowered to C_1, due to an out-of-plane rotation of the OH fragment by 40°. However, the C_1 structure is lower by only 0.1 kcal/mol relative to the C_s proton-transferred configuration. In the C_s symmetry saddle, the oxygen-oxygen distance is also 2.47 Å.

To benchmark the DFT methods, we have investigated how different theoretical models reproduce the relative energies of the isomers. In view of SIE, we also included the hemibonded structure predicted to be the lowest isomer by some DFT calculations (Table 4). It has (near) C_{2h} symmetry with the charge equally distributed between the fragments. Such systems are problematic for both the HF and the DFT methods. The former tends to destabilize them due to symmetry breaking, while the latter over-stabilize them due to SIE. The EOM-IP-CC methods based on the neutral reference are free from these artifacts. Table 3 compares the energies of the $(H_2O)_2^+$ isomers obtained at different levels of theory using wave function methods. These methods consistently predict the proton-transferred isomer to be lower than the hemibonded form. At the HF level, the difference between the proton-transferred and hemibonded structures is 26 kcal/mol, and electron correlation brings it down to 7-8 kcal/mol. The large difference at the HF level is due to the symmetry breaking problem at the hemibonded geometry. The energy difference between the proton-transferred and vertical configurations only weakly depends on the level of theory and is approximately 20 kcal/mol. This stable behavior is due to the charge-localized character of the wave functions, which are free from the HF instability, and are well described using both open-shell and closed-shell references.

The set of the $(H_2O)_2^+$ structures was re-optimized using DFT. The results are summarized in Table 4. The DFT calculations without SIC show the following trends. First, there is virtually no energy difference between the unrestricted and restricted open-shell BLYP results. Second, compared to the benchmark EOM-IP-CCSD calculations, BLYP overstabilizes both the vertical and the hemibonded dimer structures by -12 and -13 kcal/mol, respectively. The error for the hemibonded structure is comparable in absolute value to that of HF. However, the sign is opposite and, as was shown before,[28] the SIE uncorrected DFT erroneously places the hemibonded minimum below the proton-transfer one. This is a well-known signature of SIE observed in many systems with charge separation.[47,52,53]

A simple empirical SIC correction for doublet states based on removing SI of the unpaired electron implemented for restricted open shell BLYP,[48,49] improves the results dramatically. For the recommended choice of the two scaling parameters (0.2 and 0), the error in the above relative energies drops to 2-3 kcal/mol (compared to EOM-IP-CCSD) and is further reduced to less than 2 kcal/mol upon moving from DZVP to TZVDD basis set. This is encouraging and justifies the use of DFT/BLYP with the present SIC for condensed phase AIMD calculations.[12] Note that it is theoretically more appealing to employ twice the same value for the scaling parameters (i.e., 0.2 and 0.2), similar to other approaches,[54] but we find that this leads to worse results. The correct order of minima is preserved, but the error increases to about -4 kcal/mol.

Finally, DFT reoptimization of the proton-transfer and hemibonded structures results in minor geometry and, consequently, energy changes (Table 4). The geometry of the neutral dimer, which is not a minimum on the cationic surface, collapses to the proton-transfer minimum upon minimization (as for EOM-IP-CCSD).

The use of restricted open-shell formalism with Kohn-Sham DFT deserves an additional comment. As shown by Pople and coworkers,[55] in open-shell systems that have excess α

electrons, regions of negative spin density exist. That means, that the local density of β electrons may be higher than the density of α electrons. The local excess of β electrons is reproduced by correlated calculations, as well as confirmed experimentally. In the DFT framework, it can only be reproduced within UKS formalism, simply because the electron density is a sum of the MO densities, which are the same for both spins in ROKS. However, the SIC applied here is stable only within ROKS formalism, as it requires one to identify the unpaired electron. Modern density functionals containing non-local operators, such as long range Hartree-Fock exchange, promise to reduce the SIE in a more fundamental way.[56–59] However, symmetric radical cations are particularly difficult systems, and performance is not yet fully satisfactory.[59]

3.2.2 DMO-LCFMO framework

The dimer spectroscopy can be explained in terms of the individual fragment contributions. The theoretical framework is provided by the DMO-LCFMO theory, which was applied previously to the electronic structure of the benzene dimer cation,[15] and is described in the Appendix. It allows one to correlate the dimer and monomer transitions based on the degree of mixing of the FMOs in the dimer. We employ a (H-bond donor orbital)/(H-bond acceptor orbital) notation, allowing one to quickly discern the FMOs that contribute to a given DMO. If there is no component on the given fragment, a symbol 0 is used. An asterisk signifies antibonding character of the dimer MO with respect to the fragments interaction. The extent to which a given FMO participates in a given DMO can be quantified using the NBO analysis. NBO yields the charges of the fragments, which are related to the square of the diabatic wave function defined here as the charge-localized state. Below we discuss the DMOs at the vertical and at the proton-transferred geometry.

The orbitals at the vertical configuration are shown in Fig. 3. The SOMO is the b_1 orbital of the H-bond donor molecule, and is called $b_1/0$. It is antisymmetric with respect to the plane of symmetry. The delocalization of this orbital requires mixing with an antisymmetric orbital of the H-bond acceptor molecule. The only such orbital is $0/b_2$, which is high in energy, and, therefore, the ground state hole is localized. The two lower orbitals are linear combinations of the acceptor b_1 and the donor a_1 MOs. The higher energy combination is antibonding with respect to the monomers and is called $(a_1/b_1)^*$. The bonding combination is (a_1/b_1). Lower in energy we find the $(b_2/a_1)^*$ and (b_2/a_1) pair. The antibonding DMO is located mostly on the acceptor, while the donor hosts the bonding component. Finally, the acceptor $0/b_2$ is the lowest DMO considered here. States corresponding to ionizing the H-bond donor are lower in energy (the corresponding FMOs are higher in energy), which can be easily rationalized in terms of electrostatic interaction. A hole on the H-bond donor fragment is stabilized by the negatively charged oxygen of the acceptor, while a hole on the acceptor is destabilized by the positively charged proton.

Orbitals at the C_s and C_1 proton-transferred configurations are shown in Fig. 4. The proton transfer drastically changes the character of the MOs and it is no longer possible to diabatically correlate them with those of the neutral. The MOs clearly separate into the H_3O^+ and OH fragments. Orbitals of the hydroxyl part are higher in energy than those of H_3O^+, as follows from the difference of IEs. Under C_s symmetry, the HOMO is the out-of-plane component of the degenerate π-pair on the OH^- fragment, $\pi_{oop}/0$. Below it are the $\pi_{inp}/0$ and $\sigma/0$ DMOs. The degenerate π system follows the out-of-plane rotation of the hydroxyl

group. H_3O^+ orbitals appear in the following order: $0/a_1$, $0/e'$, and $0/e''$. The OH σ and H_3O^+ e' orbitals are slightly mixed. Overall, only minor differences are observed in the C_s and C_1 structure orbitals.

The NBO charges reveal stronger delocalization than suggested by visual inspection of the MOs. The delocalization is due the wave function having significant amplitude between the two fragments at close distances. Additionally, for the excitations from H_3O^+ to OH one might expect to see -1 charge on the hydroxyl fragment. However, the large positive charge on H_3O^{2+} will polarize the OH^- and thus decrease its charge. This is confirmed by the calculation, revealing -0.771 charge on the OH moiety.

3.2.3 Spectroscopy at the vertical configuration

Table 5 and Fig. 5 present excitation energies and transition properties of $(H_2O)_2^+$ at the geometry of the neutral species. All excitations involve transfer of an electron to the SOMO, i.e., the $b_1/0$ orbital. Overall, all theoretical methods are in good agreement in terms of energetics. A state involving excitation to a virtual orbital of the neutral appeared in the EOM-EE-CCSD calculation at 8 eV and was disregarded.

At low energies, up to ca. 2 eV, we find excitations from the $(a_1/b_1)^*$ and (a_1/b_1) pair into the SOMO. Their intensity can originate both from the intramolecular and intermolecular terms and reflects the partitioning of the DMOs into FMOs, and can be explained by DMO-LCFMO. Referring to formalism summarized in the Appendix, $(a_1/b_1)^*$ and (a_1/b_1) are examples of DMOs in which both the α and β coefficients (i.e., the weights of the FMOs) are significant. The weights of the FMOs are just the square roots of the EOM-IP-CCSD NBO charges, since both fragments are neutral in the reference state:

$$(a_1/b_1)^* = 0.355(a_1/0) - 0.935(0/b_1) \quad (3)$$

$$(a_1/b_1) = 0.886(a_1/0) + 0.464(0/b_1) \quad (4)$$

Neglecting the intermolecular contribution to the intensity, one can evaluate the transition dipole moments for the two transitions according to Eq. (7). The corresponding squares are 0.0029 and 0.0180 a.u.^{2}. This estimate is in an excellent agreement with the actual EOM-IP-CCSD dimer calculation, which yields 0.0038 and 0.0181 a.u.^{2}, thus supporting the assumption that these two transitions draw their intensity from the H-bond donor a_1 component of the DMO and that the intermolecular terms are negligible. The EOM-IP-CCSD and EOM-EE-CCSD methods predict different relative intensity of the two bands. While EOM-EE-CCSD predicts nearly equal intensities, EOM-IP-CCSD suggests 1:5 intensity ratio in favor of the higher energy band. The origins of this discrepancy can be traced back to different partitioning of the a_1 component between the $(a_1/b_1)^*$ and (a_1/b_1) pair. Our benchmark study[60] demonstrated that EOM-IP-CCSD provides a more accurate description of charge delocalization and more accurate transition properties.

EOM-IP-CCSD predicts weak excitations from the $(b_2/a_1)^*$ and (b_2/a_1) pair to be at 4 and 6.5 eV, respectively. EOM-EE-CCSD predicts the transition from the antibonding DMO to lie 0.3 eV higher and agrees as to the position of transition from the bonding DMO. The antibonding orbital is confined to the H-bond acceptor, while the bonding one — to the donor. Conceptually, the character of the transitions is similar to that discussed above. These two excitations correspond to the symmetry forbidden $b_1 \leftarrow a_1$ excitation in the monomer. Consequently, the intramolecular term in Eq. (7) is zero. Orbital relaxation and intermolecular

terms account for the intensity of these bands, which are still hundred times weaker than the allowed transitions.

Finally, around 8 eV we find the $(b_1/0) \leftarrow (0/b_2)$ transition. It is a pure charge-transfer band ($\alpha = 0$), where the hole is moved from the donor to the acceptor molecule. Its considerable intensity is due to particularly favorable overlap between the initial and final orbitals. The transition is still an order of magnitude weaker than the sum of the $(b_1/0)\leftarrow(a_1/b_1)$ and $(b_1/0)\leftarrow(a_1/b_1)^*$ excitations.

3.2.4 Spectroscopic signatures of proton transfer

Excitation energies and transition properties at the C_1 and C_s proton-transferred geometries are presented in Tables 6 and 7, respectively. The EOM-IP-CCSD data are shown in Fig. 6. We were able to obtain EOM-EE-CCSD results only for the three lowest excitations, as the states involving virtual orbitals of the neutral wave function are the next higher in energy. The lowest energy transition is at 9.6 eV, well beyond the energy range potentially probed in the experiment. Additionally, the Rydberg character of these states means that they are likely to be significantly perturbed in the condensed phase. All the excitations considered here involve the transfer of an electron to the singly occupied $(\pi_{oop}/0)$ orbital. Due to the localized character of the DMOs, the spectrum partitions into two parts: transitions within the OH fragment and transitions from the H_3O^+ to the OH fragment. In the language of the Appendix, the lower-energy part of the spectrum is close to the β=0 limit, while the higher energy one approaches the α=0 limit, i.e., local and charge transfer excitations, respectively.

The C_s and C_1 configurations differ only slightly in positions and intensities of the transitions in the low-energy part of the spectrum. The transitions in this region are from the $(\pi_{inp}/0)$ and $(\sigma/0)$ orbitals. The former excitation is not present in an isolated OH monomer, as the $(\pi_{inp}/0)$ - $(\pi_{oop}/0)$ pair is degenerate. In the dimer, it splits by 0.5 eV and acquires oscillator strength. The $(\pi_{oop}/0)\leftarrow(\sigma/0)$ excitation is at 4.5 eV, very close to the monomer value of 4.2 eV, however, its intensity is less than half. The origin of the intensity decrease can be investigated using DMO-LCFMO, although its quantitative application is complicated by the large extent of charge transfer occurring in the neutral and in the cation states. We perform the calculation for the C_s structure, but the result for the C_1 geometry is essentially identical. To obtain the singly occupied orbital, one needs to consider the difference between the neutral and the cation states (the singly occupied orbital is the same as the orbital of the outgoing electron). The NBO analysis of the CCSD wave function of the OH^- – H_3O^+ system revealed a -0.771 charge on the hydroxyl moiety. In other words, 0.916 and 0.853 electron comes from this moiety when an electron is removed from the $(\pi_{inp}/0)$ and $(\sigma/0)$ orbitals, respectively. Using these numbers to calculate the weights of the appropriate diabatic states and, subsequently, the transition dipole moment, one obtains 0.024 a.u.^{2}, almost twice the *ab initio* calculated value. The source of the discrepancy appears to be the coupling with $0/e'$ and the arising intermolecular contribution to the intensity.

Higher in energy there are excitations involving the transfer of an electron from H_3O^+ to OH. The first one, at $\sim$ 8 eV, is the transition from the lone pair $(0/a_1)$ orbital. It is very weak in the C_s structure, however, upon rotation of the hydroxyl group it acquires intensity comparable to the $(\pi_{oop}/0)\leftarrow(\sigma/0)$ transition, presumably due to the favorable overlap of the two DMOs, which increases upon rotation. In the C_s structure, the two orbitals resemble two orthogonal p orbitals. Hence, the positive and negative contributions to the transition dipole

moment cancel out. In C_1, they are akin to p_z orbitals form the π system in ethylene and all the contributions have the same sign. Above 13 eV we find excitations from $(0/e')$ and $(0/e'')$.

3.2.5 Proton transfer PES scan

Fig. 7a presents the PES scan of the proton transfer reaction in the C_s geometry. The coordinates are the oxygen-oxygen distance and the distance between the transferring proton and the accepting oxygen. Points A and C correspond to the vertical and proton-transferred geometries, respectively. They were identified based solely on the two geometric parameters scanned. The energy of point A is 3.5 kcal/mol lower than the energy at the neutral geometry due to relaxation of unconstrained coordinates. This lowers the energy change due to the reaction from 20 kcal/mol to 16.5 kcal/mol. A two-step picture of the proton transfer reaction emerges from the graph. Between points A and B, the H-bond donor molecule moves towards the acceptor, as the oxygen-oxygen and hydrogen-oxygen distances change in unison. This motion lowers the energy by 11.4 kcal/mol. Subsequent dynamics is restricted to the proton, which transfers from the donor to the acceptor, accompanied by minor adjustments in the oxygen-oxygen distance. An energy change of 5.0 kcal/mol is associated with this motion.

The PES allows us to compute the spectral changes along the steepest descent reaction path. Calculated excitation energies and transition properties are presented in Fig. 7b-d. We employ the C_s symmetry labels to identify the states in this discussion, as the character of the orbitals changes along the reaction coordinate. All the transitions involve the transfer of an electron to SOMO, the $2a''$ orbital, which is the out-of-plane orbital on the H-bond donor. Its character evolves from the H_2O^+ lone pair b_1 orbital to the π orbital of OH. Of particular interest are the $6a'$, $7a'$, and $8a'$ transitions, as they are within the spectroscopic 1 - 6 eV window. At point A, two absorption bands appear around 2 eV ($8a'$ and $7a'$). They are transitions from the bonding and antibonding combinations of the donor a_1 and acceptor b_1 fragment MOs [$(a_1/b_1)^*$ and (a_1/b_1)]. The lower energy transition carries more intensity, which is different from the fully optimized neutral configuration, where the higher energy transition carries more intensity. This is due to slightly different geometry and orbital mixing of H-bond acceptor b_1 and donor a_1 in the two states. $6a'$ and $5a'$ are bonding and antibonding combinations of donor b_2 and acceptor a_1. They are at 6.2 and 4.3 eV, respectively. The intensities of both bands are small. Finally, at 8.5 eV we find the transition from the $1a''$ (acceptor b_2) orbital.

As the reaction proceeds to point B, the intensity of $8a'$ and $7a'$ changes as the bands move apart. In other words, the partitioning of H-bond donor a_1 and acceptor b_1 in the $(a_1/b_1)^*$ and (a_1/b_1) pair changes. The small magnitude of change is easily understood within the diabatic framework of $(a_1/0)$ and $(0/b_1)$ states, i.e., the states with the charge localized on the H-bond donor and acceptor, respectively. The coupling and separation of the diabatic states increase at shorter distances. The two effects largely cancel out and no drastic changes in intensity are observed. There is a small increase in the intensity of the $6a'$ (H-bond acceptor a_1) band.

At point B, the proton transfer step starts taking place and the character of MOs changes more dramatically. The SOMO becomes the out-of-plane π orbital. The intensity of the $8a'$ band drops significantly with a decrease in energy, as it becomes a $\pi - \pi$ transition on the OH fragment. The $7a'$ excitation gains intensity as energy rises to 4.5 eV, and becomes the $\sigma - \pi$ excitation. At the same time, the $6a'$ and $5a'$ excitations move to higher energy, becoming CT excitations from H_3O^+ to OH. The already small intensity of excitation from $6a'$ drops

further as it becomes the apical orbital of H_3O^+. Both $1a''$ and $5a'$ transitions move to 12 – 14 eV, outside the experimental region.

4 Discussion

Three geometries on the ground state PES of the water dimer cation are of prime importance in the photoionization process. The first two are minima — the proton-transferred and the hemibonded structures (Fig. 2b-c). The third one is the geometry of the neutral dimer reached by vertical ionization (Fig. 2a). The geometries and relative energetics of these structures calculated by correlated electronic structure methods are in good agreement with each other (Table 3) and previous *ab initio* results.[24,25,28] All these calculation correctly characterize the proton-transferred geometry as the global minimum lying 5-10 kcal/mol below the hemibonded local minimum and about 20 kcal/mol below the structure corresponding to vertical ionization of the neutral water dimer. This ordering is reproduced already at the HF level, which, however, grossly (by about 20 kcal/mol) destabilizes the hemibonded structure due to the tendency of HF to artificially localize the MOs in systems with symmetrically equivalent centers. In contrast, the proton-transferred structure has spin localized on one fragment and charge localized on the other and in the vertical geometry, corresponding to the neutral water dimer, the spin and charge are initially localized on one water. The behavior of the DFT methods is exactly opposite. Due to SIE, DFT/BLYP overstabilizes structures with delocalized charge, and erroneously predict the hemibonded structure to be the global minimum. However, a simple a posteriori SIC,[48,49] almost completely removes this artifact and the predictions of the SIC-corrected DFT methods practically coincide with those of MP2. This is a good news for the DFT-based AIMD studies of ionization in liquid water.[12]

For ionization in the condensed phase, the issue of electronic localization/delocalization is of interest. We will address the question whether the charge is localized at one site immediately upon ionization or whether it will localize after being initially delocalized over many water molecules. This localization process can be explored by considering clusters beyond the dimer. In the dimer, the hole forms on the b_1 orbital of the H-donor fragment immediately upon ionization. This initial localization is due to the fact that the donor water is not acting as an acceptor to any other H-bond. The b_1 orbital of the H-bond acceptor in fact couples with the a_1 orbital of the donor. Neutral water dimer thus represents the most asymmetric arrangement of water molecules. Already in the cyclic trimer the water molecules become equivalent, which means that upon ionization the hole must be initially delocalized. In the bulk phase, each water molecule is likely to serve simultaneously as a hydrogen bond acceptor and donor, thus more likely delocalizing the hole. In general, small and medium-sized water clusters with different geometries will provide a natural laboratory to investigate the electronic and nuclear dynamics upon ionization with varying degree of initial localization/delocalization of the hole.[61]

Charge localization is intimately related to the electronic spectroscopy of the system. Using formalism of the Appendix, the α and β coefficients may both be significant (delocalized charge), or one can dominate (localized). Thus, excitations will have a mixed charge transfer and local character. With no knowledge of the degree of charge delocalization, it is impossible to say anything about the intensity of mixed bands and reliable *ab initio* calculations are needed. In the case of dimer cation states, one may expect intermolecular contributions to be

less significant than in their neutral counterparts due to the more compact nature of MOs. This maybe counteracted by the decreased separation manifested in a charged species. Our calculations for water dimer cation reveal that the intermolecular terms are typically an order of magnitude smaller than the intramolecular terms for allowed transitions. Note, however, that the interfragment contribution varies exponentially with the distance (separately from α and β) and may change significantly with relative orientation of the two fragments, thus allowing one to monitor the molecular dynamics via intensity and/or position of those bands.

Next, we discuss the nuclear motions along the reaction coordinate leading from the geometry corresponding to the neutral water dimer to the proton-transfer structure (Fig. 7a). The reaction, which is a downhill process without a barrier, proceeds in two steps. The first one involves heavy atom motions, i.e., the two water molecules move closer to each other with the oxygen-oxygen distance decreasing from 2.9 to 2.5 A. This step is responsible for the largest part of the energy gain ($\sim$12 kcal/mol) along the reaction coordinate. Since it involves motion of heavy atoms, it is relatively slow ($\sim$50 fs, as indicated by AIMD simulations). The second step is the transfer of the proton, which can only happen when the water oxygens are sufficiently close to each other. This process involves a motion of a light particle and is, therefore, possibly as fast as a few femtoseconds. The energy gain associated with the proton hop is smaller, amounting to roughly 5 kcal/mol. In larger cluster and in bulk liquid water, this two-step mechanism should be preserved, although it might be preceded by initial fast charge localization.[12] This is exactly the dynamics that we wish to resolve in the condensed phase, with a spectroscopic handle on these events being provided by the changing excitation spectrum of the radical species along the proton transfer reaction.

Let us consider how the electronic transitions, their band positions and their intensities, evolve as we move along the reaction coordinate. Femtosecond spectroscopy should be able to monitor the system evolution by recording changing transient absorption spectrum. Formally, the H_2O^+ cation is derived from the OH radical by the addition of a proton. One might thus expect the electronic structure and the spectroscopy of the two species to be similar. However, the results from Table 2 show that the addition of a proton is not a benign perturbation to the electronic structure. The OH radical has a characteristic absorption band around 4.2 eV corresponding to the transition of the bonding σ electron into the non-bonding π hole. Even if the proton is brought up along the O-H axis leading to a linear H-O-H^+, the σ to π promotion is pushed up to higher energy ($\sim$ 6eV). More significantly, allowing the structure to adopt the lower energy bent configuration splits the π orbital into b_1 and a_1 symmetry components. The former $\pi \leftarrow \sigma$ transition becomes dipole forbidden for the ground state component ($b_1 \leftarrow b_2$). In C_{2v}, the transition between the two formerly degenerate b_1 and a_1 orbitals is dipole allowed with a transition energy of ca. 2.3 eV and one third of the oscillator strength of the OH transition. Simply put, the 4 eV band disappears and a weaker 2.3 eV band appears in its place.

At the vertical geometry, the transitions for the ionized water dimer are perturbed and include some charge-transfer character, however, the wave functions can still be correlated with those of the monomers. Extracting the three points A, B and C from Fig. 7, we have replotted how the experimental spectrum can track the chemical reaction dynamics in Fig. 8. At A, the bands at 2 eV $(b_1/0) \leftarrow (a_1/b_1)^*$ and $(b_1/0) \leftarrow (a_1/b_1)$ [$2a'' \leftarrow 8a'$ and $2a'' \leftarrow 7a'$] have almost the same oscillator strength as the monomer. The distribution of intensity between the two heavily depends on the system geometry. The 6 eV monomer-like transition is now not strictly symmetry forbidden, particularly the 4 eV $(b_2/0) \leftarrow (b_2/a_1)^*$ [$2a'' \leftarrow 6a'$] component

with more CT character. It still is almost two orders of magnitude weaker than the 2 eV transition. Therefore, the dominant characteristic electronic absorption of the dimer cation at the Franck-Condon geometry is around 2 eV (620 nm) as for the gas phase monomer. Then at B, the $(b_2/0) \leftarrow (a_1/b_1)^*$ and $(b_2/0) \leftarrow (a_1/b_1)$ $[2a'' \leftarrow 8a'$ and $2a'' \leftarrow 7a']$ shift apart, the lower energy band carrying more intensity. The 4 eV transition shifts slightly to the blue. At this point proton transfer begins. The lower energy band becomes a weak $\pi - \pi$ excitation, while the 4 eV band gains intensity to become the $\sigma - \pi$ excitation. The shift is a clear fingerprint of the reaction and the significant change corresponds to the charge transfer between the species, i.e., from B to C. Overall, the band positions resemble the monomers, however, the intensity pattern and fine structure is a strong function of the relative geometries in the cluster. For example, the comparison of the C_s and C_1 geometries of the proton-transferred complexes show a dramatic variation in the $0/a_1$ $[6a']$ band because of the alignment of the p orbitals on the two fragments. Although C_s is a saddle point between the two equivalent C_1 configurations of the product, it is only 0.1 kcal/mol above the minima and it allows us to symmetry label the spectroscopic state of the evolving system. However, the transition to C_1 does lead to this large intensity change and one should be wary of the role of conformational changes in the band intensities. In the condensed phase, where there is an inhomogeneous distribution of conformations in the product doe to the initial water structure, this will result in conformationally averaged intensity of the band.

We are now ready to discuss the effects of bulk water. Even if the dimer core is a good representation of the vertically prepared hole in water, there is a large range of local neutral donor-acceptor geometries populated in room temperature water. Although the configuration considered is the lowest energy cluster, other configurations, particularly with different orientations of the free hydrogen of the donor with respect to the acceptor σ_v plane, should also be considered. Recent calculations have shown that, if the O-free H bond is aligned with one of the acceptor O-H bonds, the transitions with significant charge transfer character can be significantly enhanced. In particular, the band around 4 eV which involves CT $(b_2/0) \rightarrow (b_2/a_1)^*$ $[2a'' \leftarrow 7a']$ acquires oscillator strength and can become comparable to the valence band near 2.3 eV. What if more solvating waters are included around the ionized core water? Preliminary EOM-IP-CCSD computations on a pentamer extracted from ice Ih show that excitations on a central water give rise to a similar spectrum to that of the monomer with an intense band near 2 eV and little oscillator strength at 4 eV. These results will be further quantified in a subsequent study.[61]

5 Conclusions

The water dimer cation is a prototypical system for the proton transfer process in the gas and condensed phases. The vertical structure formed immediately upon ionization is not a stationary point on the cation PES and the system follows the downhill gradient to OH-H_3O^+. Our study demonstrates that this process can be monitored by femtosecond time-resolved electronic spectroscopy. At the simplest level, the initial spectrum resembles that of H_2O^+. As the reaction proceeds, band positions and intensities change. The product of the reaction spectroscopically resembles the OH radical. A more detailed look at how the electronic spectrum evolves along the proton transfer coordinate is more subtle. We observed strong coupling between the H-bond donor and acceptor orbitals, which dissolves the monomer states

into more delocalized dimer states. This coupling is likely to be present in the condensed phase as well, and will lead to significantly delocalized states. Modeling of such states requires a full quantum treatment of the entire system. Hybrid quantum mechanical/molecular mechanical methods are not appropriate for this situation as the system cannot be partitioned into a solvent and a chromophore, as, for example, in our study of electronic spectroscopy of the solvated CN radical.[62] AIMD, which is able to directly describe the electronic structure of the entire system, requires a fast electronic structure method. We have demonstrated that the energetics of $(H_2O)_2^+$ are reasonably reproduced by the ROKS-BLYP method with the simple SIC correction,[48,49] which thus can be employed in AIMD simulations of the bulk.

6 Acknowledgments

We thank Dr. C.G. Elles for discussions and helpful comments. This work was conducted under the auspices of the *iOpenShell* Center for Computational Studies of Electronic Structure and Spectroscopy of Open-Shell and Electronically Excited Species (iopenshell.usc.edu) supported by the National Science Foundation through CRIF:CRF CHE-0625419+0624602+0625237 grant. J.V. would like to acknowledge Prof. M. Sprik and Prof. J. Hutter for valuable discussions and support. P.J. acknowledges support from the Czech Ministry of Education (grant LC512) and the Granting Agency of the Czech Republic (grant 202/06/0286). S.E.B. gratefully acknowledges the support of the National Science Foundation through grant CHE-0617060.

7 Supporting Information

Optimized molecular geometries are available as supplementary materials.

8 Appendix

This section outlines the qualitative DMO-LCFMO framework for the description of the electronic states of the water dimer cation. This approach, rooted in the exciton theory,[63,64] was developed and applied to the electronic structure of the benzene dimer cation.[15] DMO-LCFMO describes the electronic wave functions of the dimer in terms of the dimer molecular orbitals expressed in the basis of the monomer MOs. This allows one to correlate properties of the dimer with the properties of the fragments. Furthermore, one need not consider the full many-electron wave function of the initial and final states, as they can be mapped onto a 1-electron-in-2-orbitals ones. The two orbitals are the orbitals involved in the transition. In the cases considered in this work, the target orbital is always the same (SOMO of the cation).

An important feature distinguishing the benzene and water systems is greater charge localization in the ground state of $(H_2O)_2^+$. The SOMO is the out-of-plane p orbital of the hydrogen bond donor, and all the considered excitation are transfers of an electron to this orbital. In the 1-electron-in-2-orbitals picture this orbital is vacant, while the other one is singly occupied.

Let us introduce a basis of three localized fragment MOs: ω_A, ν_A, λ_B, where the subscript denotes the fragment. Since one of the states in $(H_2O)_2^+$ is localized, only a single basis function on fragment B is required. A similar concept is used in molecular electronic structure, where

molecular states are described in terms of AOs. Recall, for example, $\sigma(2p_z)$ in O_2 or $\pi(p_y)$ and $\pi^*(p_y)$ in ethylene. In $(H_2O)_2^+$, we use the occupied orbitals of water monomer. We assume that the lower energy MO of the dimer is a delocalized mixture of ν_A and λ_B:

$$|\psi_1\rangle = \alpha\,|\nu_A\rangle + \beta\,|\lambda_B\rangle \tag{5}$$

where α and β satisfy the orthonormalization condition. The higher energy DMO is the localized ω_A state:

$$|\psi_2\rangle = |\omega_A\rangle\,, \tag{6}$$

This orbital represents the localized SOMO of $(H_2O)_2^+$. The transition takes place from $|\psi_1\rangle$ to $|\psi_2\rangle$. The transition dipole moment between states 1 and 2 is:

$$\langle\psi_1|\hat{\mu}|\psi_2\rangle = \alpha\,\langle\nu_A|\hat{\mu}|\omega_A\rangle + \beta\,\langle\lambda_B|\hat{\mu}|\omega_A\rangle \tag{7}$$

The equation shows that both interfragment ($\langle\lambda_B|\hat{\mu}|\omega_A\rangle$) and intrafragment ($\langle\nu_A|\hat{\mu}|\omega_A\rangle$) terms contribute to the intensity of a dimer transition. The weight of each contribution is defined by the degree of MO mixing, i.e. the α and β coefficients. Their relative phase determines whether individual contributions add or subtract. Thus, the total intensity of the monomer bands is not necessarily conserved in the dimer.

Consider first the limit of the ground state being completely localized on fragment B ($\alpha = 0$):

$$\langle\psi_1|\hat{\mu}|\psi_2\rangle = \langle\lambda_B|\hat{\mu}|\omega_A\rangle \tag{8}$$

The transition becomes a pure charge transfer excitation in which the electron moves from B to A. Its intensity may become strong when the fragments are closer together, but will decrease rapidly with the distance due to the exponential decay of the fragment wave functions. In the limit of the excited state localized on A ($\beta = 0$), we obtain:

$$\langle\psi_1|\hat{\mu}|\psi_2\rangle = \langle\nu_A|\hat{\mu}|\omega_A\rangle \tag{9}$$

Thus the excitation becomes a purely local excitation on fragment A. Within this framework,the electron density on fragment B is not affected. Its intensity is the same as in the monomer, i.e. a forbidden excitation remains forbidden and an allowed one remains allowed. However, in a dimer the orbitals and molecular geometries become distorted relative to isolated fragments and forbidden transitions often acquire small intensity.

References

[1] Sancar, A. *Biochemistry* **1994**, *33*, 2.

[2] Bixon, M. ; Jortner, J. *J. Phys. Chem. A* **2001**, *105*, 10322.

[3] Garrett, B.C. ; Dixon, D.A. ; Camaioni, D.M. ; Chipman, D.M. ; Johnson, M.A. ; Jonah, C.D. ; Kimmel, G.A. ; Miller, J.H. ; Rescigno, T.N. ; Rossky, P.J. ; Xantheas, S.S. ; Colson, S.D. ; Laufer, A.H. ; Ray, D. ; Barbara, P.F. ; Bartels, D.M. ; Becker, K.H. ; Bowen, H. ; Bradforth, S.E. ; Carmichael, I. ; Coe, J.V. ; Corrales, L.R. ; Cowin, J.P. ; Dupuis, M. ; Eisenthal, K.B. ; Franz, J.A. ; Gutowski, M.S. ; Jordan, K.D. ; Kay, B.D. ; JA, J.A. LaVerne ; Lymar, S.V. ; Madey, T.E. ; McCurdy, C.W. ; Meisel, D. ; Mukamel, S. ; Nilsson, A.R. ; Orlando, T.M. ; Petrik, N.G. ; Pimblott, S.M. ; Rustad, J.R. ; Schenter, G.K. ; Singer, S.J. ; Tokmakoff, A. ; Wang, L.S. ; Wittig, C. ; Zwier, T.S. *Chem. Rev.* **2005**, *105*, 355.

[4] Elles, C.G. ; Jailaubekov, A.E. ; Crowell, R.A. ; Bradforth, S.E. *J. Chem. Phys.* **2006**, *125*, 44515.

[5] Elles, C.G. ; Shkrob, I.A. ; Crowell, R.A. ; Bradforth, S.E. *J. Chem. Phys.* **2007**, *126*, 64503.

[6] Schnitker, Jürgen ; Rossky, P.J. *J. Chem. Phys.* **1987**, *86*, 3471.

[7] Boero, M. ; Parrinello, M. ; Terakura, K. ; Ikeshoji, T. ; ; Liew, C.C. *Phys. Rev. Lett.* **2003**, *90*, 226403.

[8] Tachikawa, Hiroto *J. Phys. Chem. A* **2004**, *108*, 7853.

[9] Tachikawa, H. *J. Phys. Chem. A* **2002**, *106*, 6915.

[10] Furuhama, A. ; Dupuis, M. ; Hirao, K. *J. Chem. Phys.* **2006**, *124*, 164310.

[11] Novakovskaya, Y.V. *Int. J. Quant. Chem.* **2007**, *107*, 2763.

[12] VandeVondele, J. ; Pieniazek, P.A. ; Krylov, A.I. ; Bradforth, S.E. ; Jungwirth, P. *to be published.*

[13] Nielsen, S. O. ; Michael, B.D. ; Hart, E.J. *J. Phys. Chem.* **1976**, *2482*, 80.

[14] VandeVondele, J. ; Sprik, M. *Phys. Chem. Chem. Phys.* **2005**, *7*, 1363.

[15] Pieniazek, P.A. ; Krylov, A.I. ; Bradforth, S.E. *J. Chem. Phys.* **2007**, *127*, 044317.

[16] Ng, C.Y. ; Trevor, D.J. ; Tiedemann, P.W. ; Ceyer, S.T. ; Kronebusch, P.L. ; Mahan, B.H. ; Lee, Y.T. *J. Chem. Phys.* **1977**, *67*, 4235.

[17] de Visser, S. P. ; de Koning, L.J. ; Nibbering, N.M.M. *J. Phys. Chem.* **1995**, *99*, 15444.

[18] S. Tomoda, Y. Achiba ; Kimura, K. *Chem. Phys. Lett.* **1982**, *87*, 197.

[19] Moncrieff, D. ; Hillier, I.H. ; Saunders, V.R. *Chem. Phys. Lett.* **1982**, *89*, 447.

[20] Sato, K. ; Tomoda, S. ; Kimura, K. *Chem. Phys. Lett.* **1983**, *95*, 579.

[21] Curtiss, L.A. *Chem. Phys. Lett.* **1983**, *96*, 442.

[22] Tomoda, S. ; Kimura, K. *Chem. Phys.* **1983**, *82*, 215.

[23] Curtiss, L.A. *Chem. Phys. Lett.* **1984**, *112*, 409.

[24] Gill, P.M.W. ; Radom, L. *J. Am. Chem. Soc.* **1988**, *110*, 4931.

[25] Sodupe, M. ; Oliva, A. ; Bertran, J. *J. Am. Chem. Soc.* **1994**, *116*, 8249.

[26] Barnett, R.N. ; Landman, U. *J. Phys. Chem.* **1995**, *99*, 17305.

[27] Barnett, R.N. ; Landman, U. *J. Phys. Chem. A* **1997**, *107*, 2763.

[28] Sodupe, M. ; Bertran, J. ; Rodrguez-Santiago, L. ; Baerends, E.J. *J. Phys. Chem. A* **1999**, *103*, 166.

[29] Müller, I.B. ; Cederbaum, L.S. *J. Chem. Phys.* **2006**, *125*, 204305.

[30] Löwdin, P.O. *Rev. Mod. Phys.* **1963**, *35*, 496.

[31] Davidson, E.R. ; Borden, W.T. *J. Phys. Chem.* **1983**, *87*, 4783.

[32] Russ, N.J. ; Crawford, T.D. ; Tschumper, G.S. *J. Chem. Phys.* **2005**, *120*, 7298.

[33] Sinha, D. ; Mukhopadhyay, D. ; Mukherjee, D. *Chem. Phys. Lett.* **1986**, *129*, 369.

[34] Sinha, D. ; Mukhopadhya, D. ; Chaudhuri, R. ; Mukherjee, D. *Chem. Phys. Lett.* **1989**, *154*, 544.

[35] Chaudhuri, R. ; Mukhopadhyay, D. ; Mukherjee, D. *Chem. Phys. Lett.* **1989**, *162*, 393.

[36] Stanton, J.F. ; Gauss, J. *J. Chem. Phys.* **1999**, *111*, 8785.

[37] Sekino, H. ; Bartlett, R.J. *Int. J. Quant. Chem. Symp.* **1984**, *18*, 255.

[38] Koch, H. ; Jensen, H.J.Aa. ; Jørgensen, P. ; Helgaker, T. *J. Chem. Phys.* **1990**, *93*, 3345.

[39] Stanton, J.F. ; Bartlett, R.J. *J. Chem. Phys.* **1993**, *98*, 7029.

[40] NBO 5.0. Glendening, E.D. ; Badenhoop, J.K. ; Reed, A.E. ; Carpenter, J.E. ; Bohmann, J.A. ; Morales, C.M. ; Weinhold, F. Theoretical Chemistry Institute, University of Wisconsin, Madison, WI, **2001**.

[41] Shao, Y. ; Molnar, L.F. ; Jung, Y. ; Kussmann, J. ; Ochsenfeld, C. ; Brown, S. ; Gilbert, A.T.B. ; Slipchenko, L.V. ; Levchenko, S.V. ; O'Neil, D. P. ; Distasio Jr., R.A. ; Lochan, R.C. ; Wang, T. ; Beran, G.J.O. ; Besley, N.A. ; Herbert, J.M. ; Lin, C.Y. ; Van Voorhis, T. ; Chien, S.H. ; Sodt, A. ; Steele, R.P. ; Rassolov, V. A. ; Maslen, P. ; Korambath, P.P. ; Adamson, R.D. ; Austin, B. ; Baker, J. ; Bird, E.F.C. ; Daschel, H. ; Doerksen, R.J. ; Drew, A. ; Dunietz, B.D. ; Dutoi, A.D. ; Furlani, T.R. ; Gwaltney, S.R. ; Heyden, A. ; Hirata, S. ; Hsu, C.-P. ; Kedziora, G.S. ; Khalliulin, R.Z. ; Klunziger, P. ; Lee,

A.M. ; Liang, W.Z. ; Lotan, I. ; Nair, N. ; Peters, B. ; Proynov, E.I. ; Pieniazek, P.A. ; Rhee, Y.M. ; Ritchie, J. ; Rosta, E. ; Sherrill, C.D. ; Simmonett, A.C. ; Subotnik, J.E. ; Woodcock III, H.L. ; Zhang, W. ; Bell, A.T. ; Chakraborty, A.K. ; Chipman, D.M. ; Keil, F.J. ; Warshel, A. ; Herhe, W.J. ; Schaefer III, H.F. ; Kong, J. ; Krylov, A.I. ; Gill, P.M.W. ; Head-Gordon, M. *Phys. Chem. Chem. Phys.* **2006**, *8*, 3172.

[42] Basis sets were obtained from the Extensible Computational Chemistry Environment Basis Set Database, Version , as developed and distributed by the Molecular Science Computing Facility, Environmental and Molecular Sciences Laboratory which is part of the Pacific Northwest Laboratory, P.O. Box 999, Richland, Washington 99352, USA, and funded by the U.S. Department of Energy. The Pacific Northwest Laboratory is a multi-program laboratory operated by Battelle Memorial Institute for the U.S. Department of Energy under contract DE-AC06-76RLO 1830. Contact David Feller or Karen Schuchardt for further information.

[43] VandeVondele, J. ; Krack, M. ; Mohamed, F. ; Parrinello, M. ; Chassaing, T. ; J, J. Hutter *Comp. Phys. Comm.* **2005**, *167*, 103.

[44] Goedecker, S. ; Teter, M. ; Hutter, J. *Phys. Rev. B* **1996**.

[45] Zhang, Y. ; Yang, W. *J. Chem. Phys.* **1998**, *109*, 2604.

[46] Polo, V. ; Kraka, E. ; Cremer, D. *Molecular Physics* **2002**, *100*, 1771 .

[47] Lundber, M. ; Siegbahn, P.E.M. *J. Chem. Phys.* **2005**, *122*, 1.

[48] d'Avezac, M. ; Calandra, M. ; Mauri, F. *Phys. Rev. B* **2005**, *71*, 205210.

[49] VandeVondele, J. ; Sprik, M. *Phys. Chem. Chem. Phys.* **2005**, *7*, 1363.

[50] Mantz, Y.A. ; Gervasio, F.L. ; Laino, T. ; Parrinello, M. *J. Phys. Chem. A* **2007**, *111*, 105.

[51] Cheng, B.-M. ; Chew, E.P. ; Liu, C.-P. ; Bahou, M. ; Lee, Y.-P. ; Yung, Y.L. ; Gerstell, M.F. *Geophys. Res. Lett.* **1999**, *26*, 3657.

[52] Bally, T. ; Sastry, G.N. *J. Phys. Chem. A* **1997**, *101*, 7923.

[53] Vanovschi, V. ; Krylov, A.I. ; Wenthold, P.G. *Theor. Chim. Acta* **2007;** in press.

[54] Vydrov, O.A. ; Scuseria, G.E. *J. Chem. Phys.* **2006**, *124*, 191101.

[55] Pople, J.A. ; Gill, P.M.W. ; Handy, N.C. *Int. J. Quantum Chem.* **1995**, *56*, 303.

[56] Tawada, Y. ; Tsuneda, T. ; Yanagisawa, S. ; T, T. Yanai ; Hirao, K.K. *J. Chem. Phys.* **2004**, *120*, 8425.

[57] Cohenand, A.J. ; Mori-Sánchez, P. ; Yang, W. *J. Chem. Phys.* **2007**, *126*, 191109.

[58] Becke, A.D. ; Johnson, E.R. *J. Chem. Phys.* **2007**, *127*, 124108.

[59] Chai, J.-D. ; Head-Gordon, M. *J. Chem. Phys.* **2008**, *128*, 084106.

[60] Pieniazek, P.A. ; Arnstein, S.A. ; Bradforth, S.E. ; Krylov, A.I. ; Sherrill, C.D. *J. Chem. Phys.* **2007**, *127*, 164110.

[61] Sundstrom, E.J. ; Pieniazek, P.A. ; Bradforth, S.E. ; Krylov, A.I. *to be published* **2008**.

[62] Pieniazek, P.A. ; Bradforth, S.E. ; Krylov, A.I. *J. Phys. Chem. A* **2006**, *110*, 4854.

[63] Birks, J.B. *Photophysics of Aromatic Molecules;* Wiley: New York, 1970.

[64] East, A.L.L. ; Lim, E.C. *J. Chem. Phys.* **2000**, *113,*, 8981.

[65] Banna, M.S. ; McQuaide, B.H. ; Malutzki, R. ; Schmidt, V. *J. Chem. Phys.* **1986**, *84*.

[66] Reutt, J.E. ; Wang, L.S. ; Lee, Y.T. ; Shirley, D.A. *J. Chem. Phys.* **1986**, *85*, 6928.

[67] Hotop, H. ; Patterson, T.A. ; Lineberger, W.C. *J. Chem. Phys.* **1974**, *60*, 1806.

[68] Smith, J.R ; Kim, J.B. ; Lineberger, W.C. *Phys. Rev. A* **1997**, *55*, 2036.

[69] Das, B. ; Farley, J.W. *J. Chem. Phys.* **1991**, *95*, 8809.

[70] Constants of diatomic molecules (data prepared by J.W. Gallagher and R.D. Johnson, III). Huber, K.P. ; Herzberg, G. NIST Chemistry WebBook, NIST Standard Reference Database Number 69; Eds. P.J. Linstrom and W.G. Mallard, July 2001, National Institute of Standards and Technology, Gaithersburg MD, 20899 (http://webbook.nist.gov).

Table 1: Ionization energies (eV) of H_2O, OH^-, and H_3O^+.

	EOM-IP-CCSD		EOM-IP-CC(2,3)		Exp.
	6-311++G**	aug-cc-pVTZ	6-311++G**	aug-cc-pVTZ	
			H_2O		
$1b_1$	12.32	12.61	12.29	12.51	12.6[a], 12.62[b]
$3a_1$	14.61	14.87	14.57	14.78	14.8[a], 14.64[b]
$1b_2$	18.84	18.94	18.78	18.83	18.6[a], 18.6[b]
			OH^-		
π	1.37	1.77	1.17	1.48	1.83[c]
σ	5.60	5.90	5.37	5.59	-
			H_3O^+		
a_1	24.38	24.64	24.41	24.61	-
e	30.16	30.25	30.17	30.21	-

[a] Ref.[65]

[b] Ref.[66]

[c] Ref.[67,68]

Table 2: Excitation energies (eV) and transition properties (a.u.) of H_2O^+, OH, and H_3O^{2+}.

	EOM-IP-CCSD			EOM-EE-CCSD			EOM-IP-CC(2,3)	exp.
	E_{ex}	μ^2	f	E_{ex}	μ^2	f	E_{ex}	E_{ex}
	H_2O^+ at the geometry of the neutral							
$3a_1$-$1b_1$	2.29	0.0229	0.00128	2.29	0.0225	0.00126	2.28	2.02 [a]
$1b_2$-$1b_1$	6.52	-	-	6.48	-	-	6.49	6.0 [a]
	H_2O^+ at the geometry of the cation							
$3a_1$-$1b_1$	2.02	0.0179	0.000885	2.01	0.0177	0.000874	2.01	1.89[b]
$1b_2$-$1b_1$	6.53	-	-	6.89	-	-	6.49 -	
	OH at the geometry of the neutral							
σ-π [a]	4.22	0.0301	0.00312	4.21	0.0311	0.00321	4.20	4.12[c]
	H_3O^{2+} at the geometry of H_3O^+							
a_1-e [b]	5.78	$6.7\ 10^{-6}$	$9.5\ 10^{-7}$	5.74	$2.5\ 10^{-5}$	$3.4\ 10^{-6}$	5.75	-

[a] Computed as a difference of vertical IEs from Ref.[66]

[b] Ref.[69]

[c] Ref.[70]

Table 3: Energies (kcal/mol) of $(H_2O)_2^+$ relative to the proton-transferred geometry calculated using wave function based methods.

	hemibonded	vertical neutral
HF	26.8	20.1
MP2	7.4	21.4
CCSD	9.9	21.4
CCSD(T)	8.2	21.6
EOM-IP-CCSD	5.3	20.0
EOM-IP-CC(2,3)	7.4	21.8

Table 4: Energies (kcal/mol) of $(H_2O)_2^+$ relative to the proton-transferred geometry calculated using DFT methods.

	hemibonded	vertical neutral
EOM-IP-CCSD geometry		
UBLYP/DZVP	-8.3	6.7
ROBLYP/DZVP	-8.3	6.6
SIC(0.2/0.0)-ROBLYP/DZVP	7.3	21.1
SIC(0.2/0.0)-ROBLYP/TZVDD	6.6	19.9
SIC(0.2/0.2)-ROBLYP/DZVP	1.0	15.0
optimized geometry		
UBLYP/DZVP	-8.8	pt
ROBLYP/DZVP	-8.7	pt
SIC(0.2/0.0)-ROBLYP/DZVP (cp2k)	7.7	pt
SIC(0.2/0.0)-ROBLYP/TZVDD	8.0	pt
SIC(0.2/0.2)-ROBLYP/DZVP	0.8	pt

Table 5: Excitation energies (eV) and transtion properties (a.u.) of the $(H_2O)_2^+$ cation at the geometry of the neutral. All transitions are to the $2a''$ ($b_1/0$) orbital. 6-311++G** basis set was used in the calculation.

		EOM-IP-CCSD			EOM-EE-CCSD			EOM-IP-CC(2,3)
		E_{ex}	μ^2	f	E_{ex}	μ^2	f	E_{ex}
$8a'$	$(a_1/b_1)^*$	1.50	0.00379	$1.39\ 10^{-4}$	1.81	0.00995	$4.41\ 10^{-4}$	1.48
$7a'$	a_1/b_1	2.25	0.0181	$9.98\ 10^{-4}$	2.37	0.0122	$7.06\ 10^{-4}$	2.23
$6a'$	$(b_2/a_1)^*$	3.99	$6.95\ 10^{-4}$	$6.80\ 10^{-5}$	4.34	$1.69\ 10^{-4}$	$1.80\ 10^{-5}$	3.97
$5a'$	b_2/a_1	6.57	$7.29\ 10^{-6}$	$1.12\ 10^{-6}$	6.56	$1.65\ 10^{-5}$	$2.65\ 10^{-6}$	6.52
$1a''$	$0/b_2$	8.07	0.00362	$7.16\ 10^{-4}$	8.46	0.00183	$3.80\ 10^{-4}$	8.04

Table 6: Excitation energies (eV) and transtion properties (a.u.) of the $(H_2O)_2^+$ cation at the C_1 proton-transferred geometry. All transitions are to the $10a_1$ ($\pi_{oop}/0$) orbital.

		EOM-IP-CCSD			EOM-EE-CCSD		
		E_{ex}	μ^2	f	E_{ex}	μ^2	f
$9a_1$	$\pi_{inp}/0$	0.49	0.00190	$2.28\ 10^{-5}$	0.49	0.00220	$2.66\ 10^{-5}$
$8a_1$	$\sigma/0$	4.52	0.0136	0.00151	4.53	0.0129	0.00143
$7a_1$	$0/a_1$	8.35	0.0141	0.00289	8.87	0.00957	0.00208
$6a_1$	$0/e'$	13.05	0.00194	$6.21\ 10^{-4}$	-	-	-
$5a_1$	$0/e''$	14.34	0.00224	$7.86\ 10^{-4}$	-	-	-

Table 7: Excitation energies (eV) and transtion properties (a.u.) of the $(H_2O)_2^+$ cation at the C_s proton-transferred geometry. All transitions are to the $10a_1$ ($\pi_{oop}/0$) orbital.

		EOM-IP-CCSD			EOM-EE-CCSD		
		E_{ex}	μ^2	f	E_{ex}	μ^2	f
$8a'$	$\pi_{oop}/0$	0.46	0.00176	$2.01\ 10^{-5}$	0.50	0.00217	$2.50\ 10^{-5}$
$7a'$	$\sigma/0$	4.48	0.0138	0.00151	4.49	0.0132	0.00145
$6a'$	$0/a_1$	8.39	$3.11\ 10^{-5}$	$6.40\ 10^{-6}$	8.95	$1.13\ 10^{-5}$	$2.47\ 10^{-6}$
$5a'$	$0/e'$	13.03	$7.07\ 10^{-4}$	$2.26\ 10^{-4}$	-	-	-
$4a''$	$0/e''$	14.31	0.00593	0.00208	-	-	-

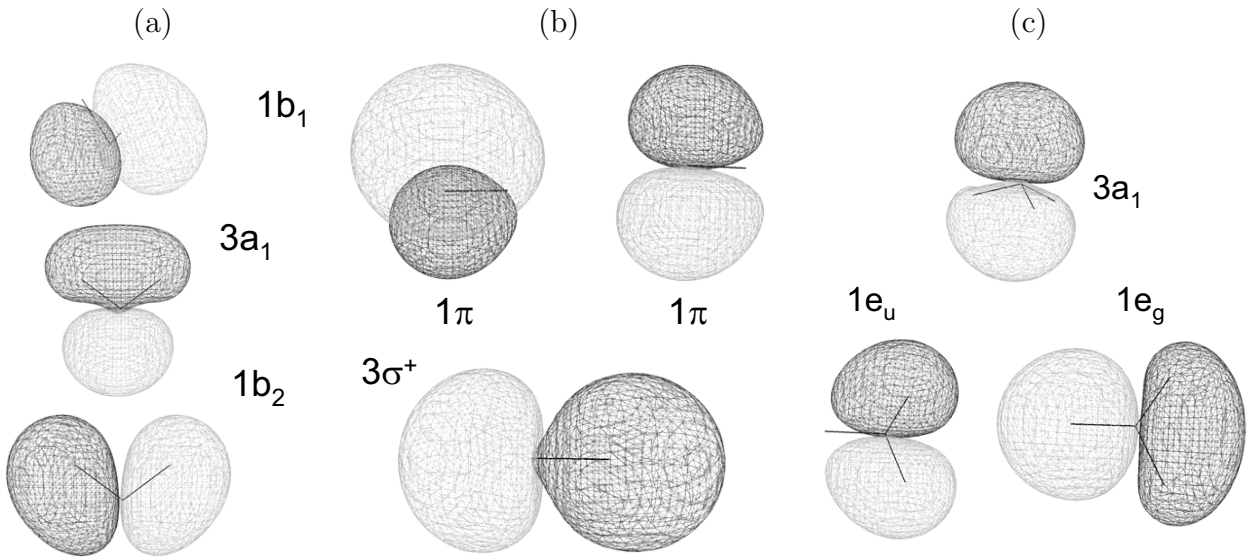

Figure 1: Three highest occupied MOs of (a) H_2O, (b) OH^-, and (c) H_3O^+. The geometric frame is rotated for each orbital to best show the orbital character.

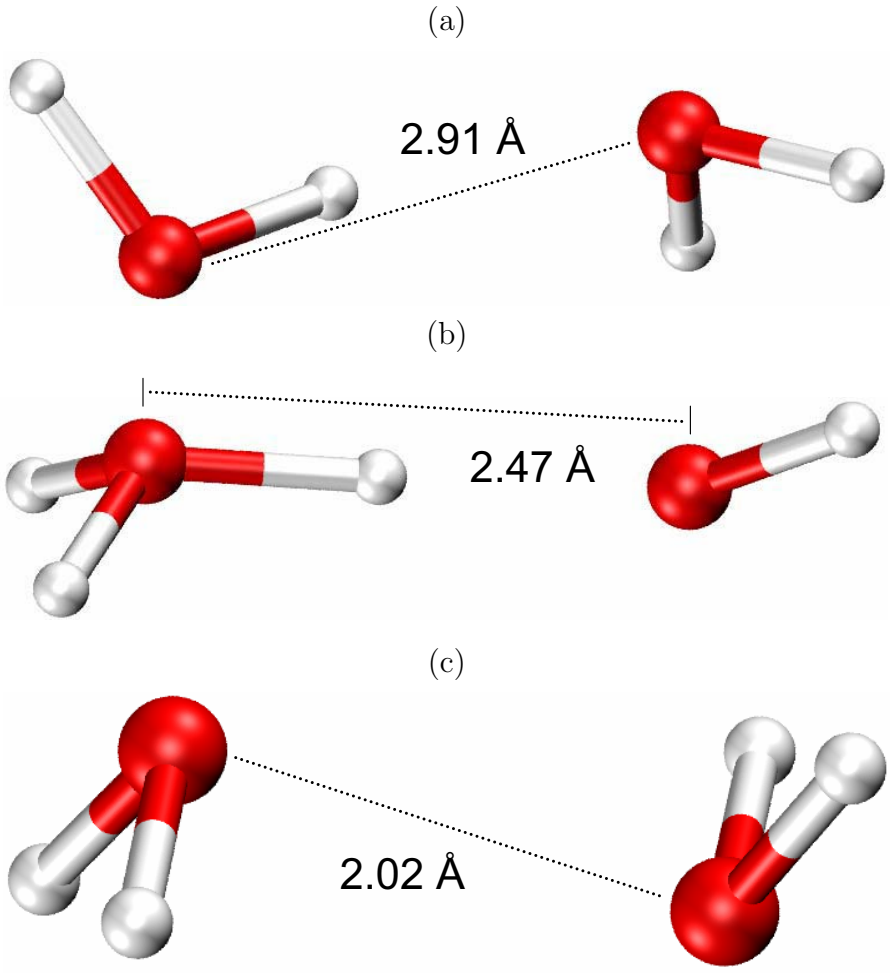

Figure 2: Geometries of (a) vertical neutral $(H_2O)_2$, (b) proton-transferred $(H_2O)_2^+$, and (c) hemibonded$(H_2O)_2^+$. Oxygen-oxygen distance has been marked on the plots.

.

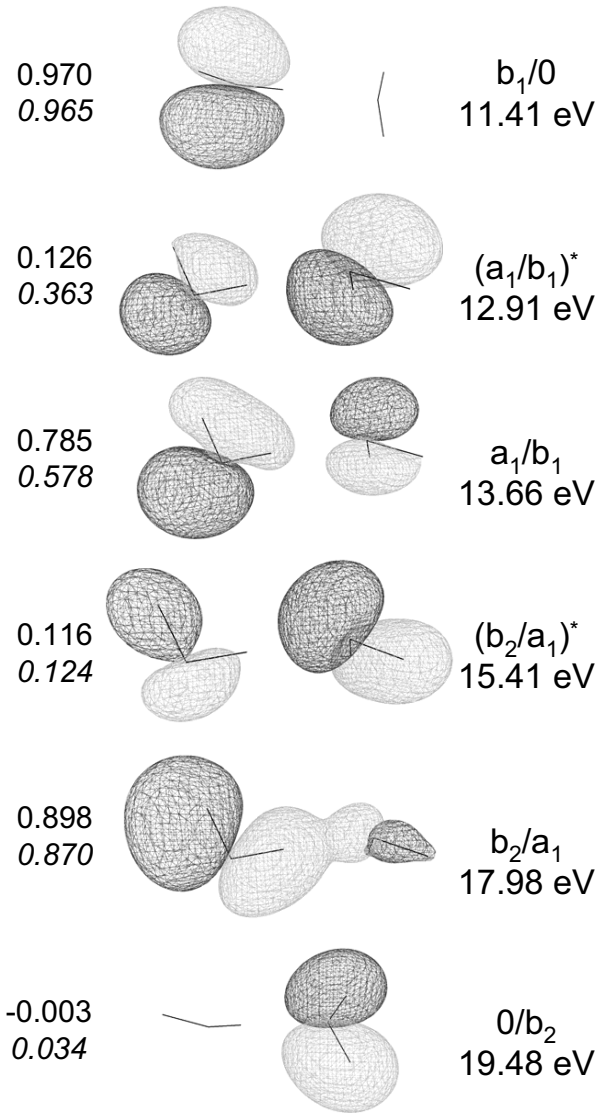

Figure 3: Six highest occupied MOs of the neutral water dimer. Ionization energies were calculated using EOM-IP-CCSD/6-311++G**. The numbers on the left are the NBO charge on the H-bond donor fragment calculated using EOM-IP-CCSD (upper number) and CCSD/EOM-EE-CCSD (lower number) wave functions. The geometric frame is rotated for each orbital to best show orbital character. The NBO analysis of the reference CCSD/6-311++G** wave function showed -0.012 charge on the H-bond donor.

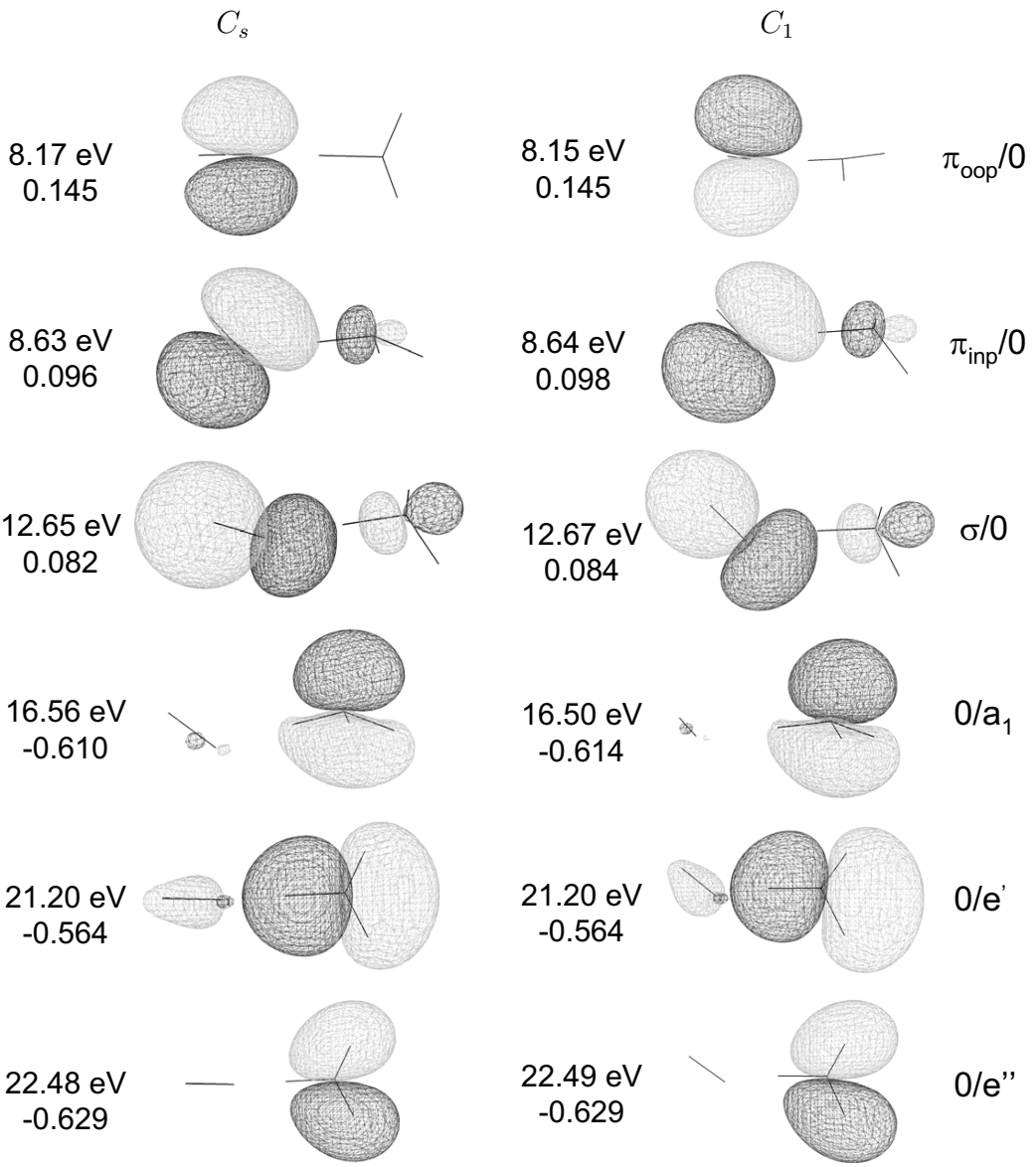

Figure 4: Six highest occupied MOs of the neutral water dimer at the C_s and C_1 proton-transferred configurations. Ionization energies were calculated using EOM-IP-CCSD/6-311++G**. The NBO charge on the hydroxyl radical calculated using EOM-IP-CCSD wave functions is given below. The geometric frame is rotated for each orbital to best show orbital character. The NBO analysis of the reference CCSD/6-311++G** wave function showed -0.771 and -0.770 charge on the hydroxyl radical in the C_s and C_1 structures, respectively.

(a)

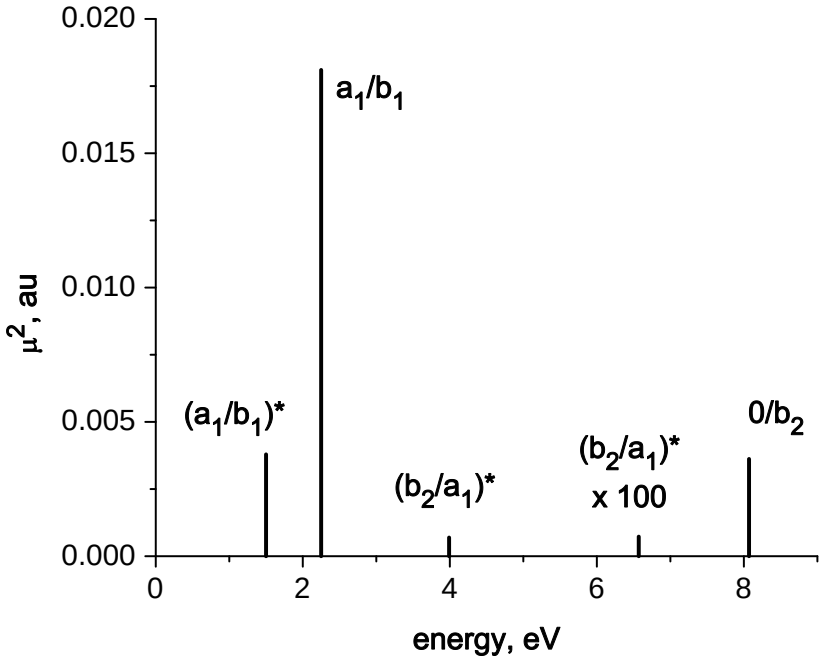

(b)

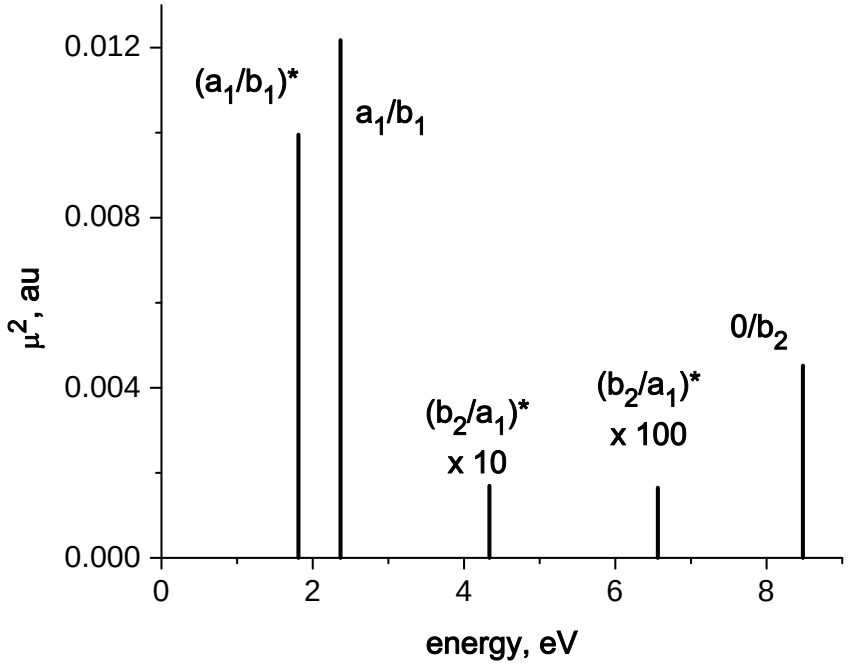

Figure 5: Electronic states ordering and transition dipole moments of water dimer cation at the neutral configuration calculated using (a) EOM-IP-CCSD/6-311++G** and (b) EOM-EE-CCSD/6-311++G** . All transitions are to the $b_1/0$ orbital.

.

(a)

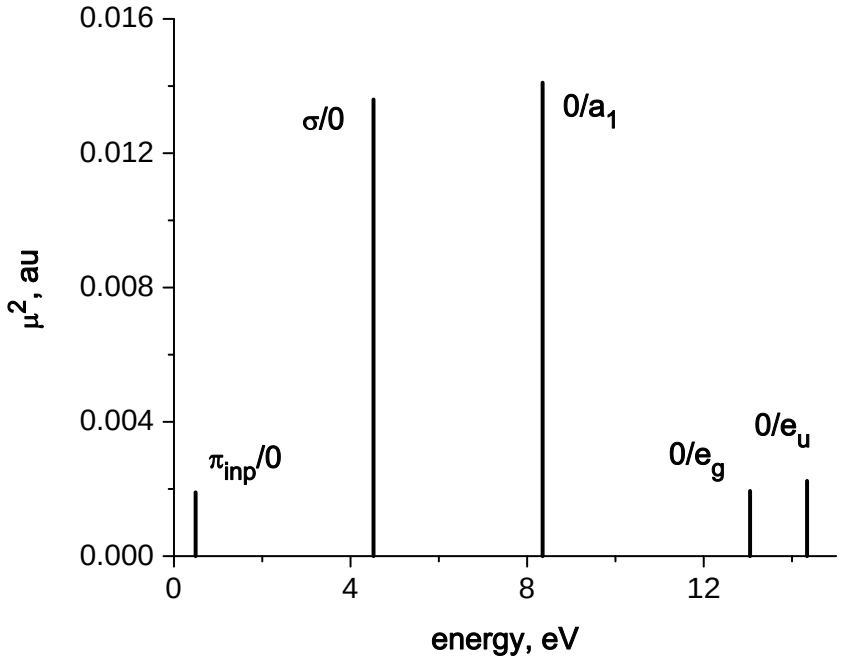

(b)

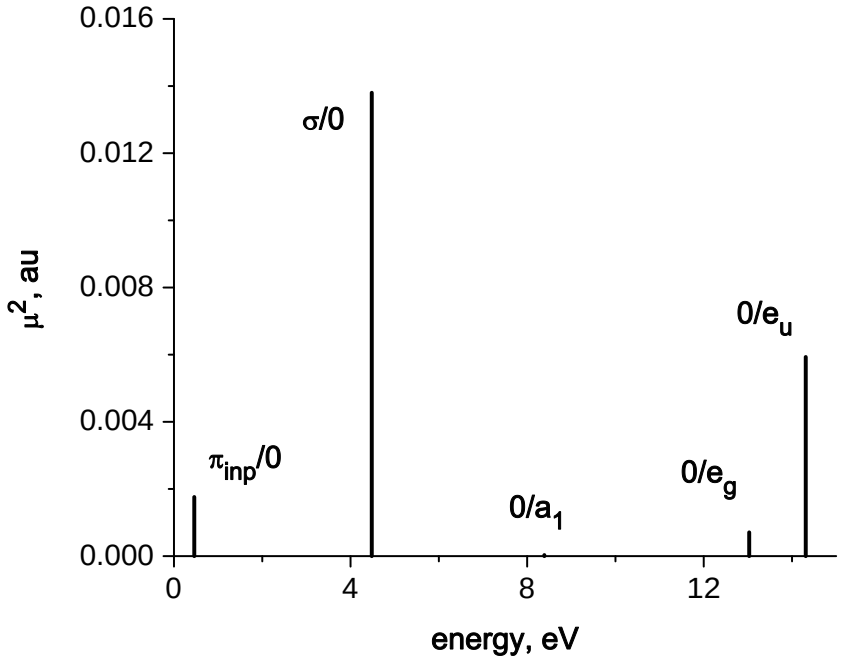

Figure 6: Electronic states ordering and transition dipole moments of water dimer cation at the C_1 (a) and C_s symmetry proton-transferred configurations calculated using EOM-IP-CCSD/6-311++G**. All transitions are to the $\pi_{oop}/0$ orbital.

.

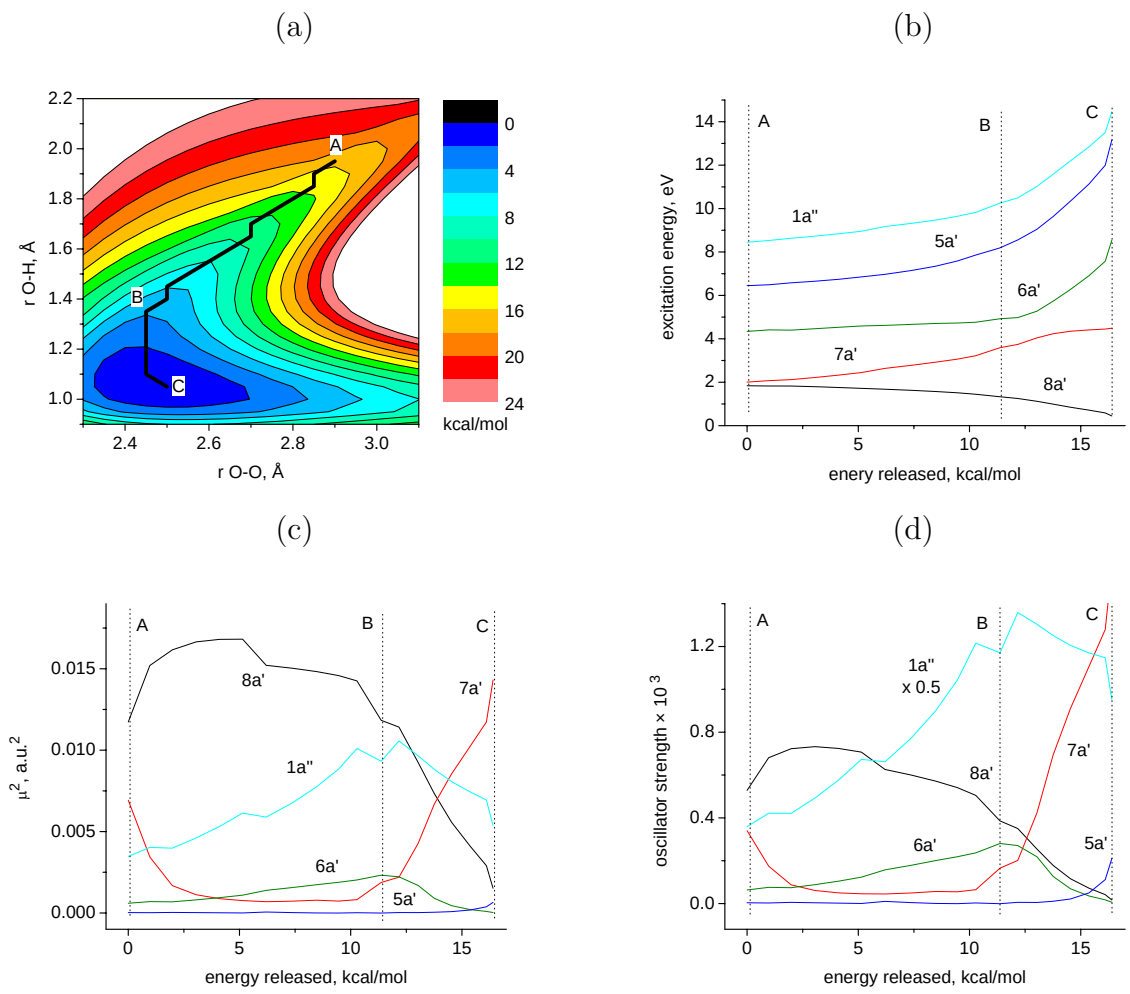

Figure 7: (a) The ground state PES scan for the proton transfer reaction. The x-axis is the oxygen-oxygen distance and the y-axis is the distance between the transferring proton and the accepting oxygen. Points A and C correspond to the neutral and proton transferred geometries, respectively. The black line is the steepest descent path. (b) -(d) Vertical excitation energies, transition dipole moments and oscillator strengths along the reaction coordinate.

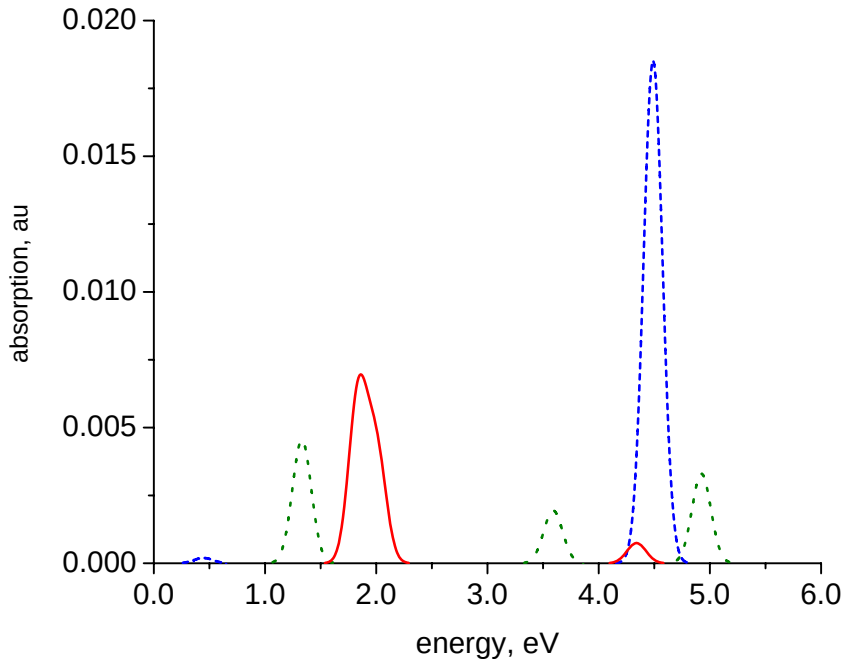

Figure 8: Evolution of the electronic spectrum of the water dimer cation along the reaction path at points A (red solid line), B (green dotted line), and C (blue dashed line). Points A and C correspond to vertical neutral and proton-transferred geometries. 0.2 eV full width at half-maximum was assumed. See Fig. 7 for details.